HHS Public Access

Author manuscript

J Invest Dermatol. Author manuscript; available in PMC 2018 February 13.

Published in final edited form as:

J Invest Dermatol. 2017 August ; 137(8): 1774–1783. doi:10.1016/j.jid.2017.03.034.

Activation of Parathyroid Hormone 2 Receptor Induces Decorin Expression and Promotes Wound Repair

Emi Sato[1], **Ling-juan Zhang**[1], **Robert A. Dorschner**[1], **Christopher A. Adase**[1], **Biswa P. Choudhury**[2], and **Richard L. Gallo**[1]

[1]Department of Dermatology, University of California–San Diego, La Jolla, California, USA

[2]Glycotechnology Core Resource, University of California–San Diego, La Jolla, California, USA

Abstract

In this study, we report that TIP39, a parathyroid hormone ligand family member that was recently identified to be expressed in the skin, can induce decorin expression and enhance wound repair. Topical treatment of mice with TIP39 accelerated wound repair, whereas TIP39-deficient mice had delayed repair that was associated with formation of abnormal collagen bundles. To study the potential mechanism responsible for the action of TIP39 in the dermis, fibroblasts were cultured in three-dimensional collagen gels, a process that results in enhanced decorin expression unless activated to differentiate to adipocytes, whereupon these cells reduce expression of several proteoglycans, including decorin. Small interfering RNA-mediated silencing of parathyroid hormone 2 receptor (PTH2R), the receptor for TIP39, suppressed the expression of extracellular matrix-related genes, including decorin, collagens, fibronectin, and matrix metalloproteases. Skin wounds in TIP39$^{-/-}$ mice had decreased decorin expression, and addition of TIP39 to cultured fibroblasts induced decorin and increased phosphorylation and nuclear translocation of CREB. Fibroblasts differentiated to adipocytes and treated with TIP39 also showed increased decorin and production of chondroitin sulfate. Furthermore, the skin of PTH2R$^{-/-}$ mice showed abnormal extracellular matrix structure, decreased decorin expression, and skin hardness. Thus, the TIP39-PTH2R system appears to be a previously unrecognized mechanism for regulation of extracellular matrix formation and wound repair.

Correspondence: Richard L. Gallo, Department of Dermatology, University of California–San Diego, 9500 Gillman Drive, #0869, La Jolla, California 92093, USA. rgallo@ucsd.edu.

AUTHOR CONTRIBUTIONS

ES designed and performed most of the experiments and wrote the manuscript. CAA assisted with RNA sequencing analysis, BPC assisted with high-performance liquid chromatography analysis, RAD assisted with the splinted-wound model, and LZ gave total experiment technical assistance and reviewed the manuscript. RLG supervised and designed experiments and wrote and prepared the manuscript. All authors reviewed and approved the final version of the manuscript.

SUPPLEMENTARY MATERIAL

Supplementary material is linked to the online version of the paper at www.jidonline.org, and at http://dx.doi.org/10.1016/j.jid.2017.03.034.

CONFLICT OF INTEREST

Currently, RLG is a consultant and has equity interest in MatriSys and Sente, Inc.

INTRODUCTION

The extracellular matrix (ECM) contains fibrillar collagens, glycosaminoglycans (GAGs), and proteoglycans (PGs), and it provides support and anchorage for cells. It regulates cell polarity, differentiation, and adhesion; protects against infection and UV light damage; and supports wound healing (Gallo et al., 1994; Naylor et al., 2011; Rostand and Esko, 1997; Trowbridge and Gallo, 2002). In the skin, the main source of ECM is thought to be dermal fibroblasts, but a recent study suggests that adipocytes also regulate ECM and may influence wound healing (Schmidt and Horsley, 2013). Decorin is a major ECM macromolecule and a member of the widely distributed small leucine-rich PG family. It is thought to have important functions in tissue assembly (Danielson et al., 1997). The common features of this family are core proteins containing two cysteine clusters flanking a leucine-rich repeat domain and the presence of an ear-repeat C-terminal motif (Schaefer and Schaefer, 2010). Decorin bears one dermatan sulfate or chondroitin sulfate (CS) side chain in the N-terminal region.

Decorin is notable as a regulator of collagen fibrillogenesis through its interaction with collagen triple helices to regulate their spacing within a fibril (Edwards, 2012; Weber et al., 1996). We previously reported that switching fibroblasts from growth on type I collagen in a monolayer to a three-dimensional (3D) collagen gel induced decorin expression (Lee et al., 2004). Mice harboring a targeted disruption of the decorin gene are viable but have fragile skin with markedly reduced tensile strength (Danielson et al., 1997). These phenomena suggest that decorin may have important roles in the proliferative and remodeling phases of wound healing, because new collagen fibrils are secreted from fibroblasts to make a strong scar during these phases (Brett, 2008). Decorin-deficient mice have been shown to have abnormal wound repair, which supports this conclusion (Jarvelainen et al., 2006).

TIP39 is a member of the parathyroid hormone (PTH) ligand family and an agonist of the PTH2 receptor (PTH2R). PTH2R is a class B G protein-coupled receptor (Usdin et al., 1999), which can stimulate both the $G\alpha_s$–adenylyl cyclase and $G\alpha_q$–phospholipase C pathways (Ritter and Hall, 2009). PTH, another PTH2R agonist, phosphorylates CREB (Atfi and Baron, 2010; Qiu et al., 2010), and phosphorylation of CREB induces decorin transcription (Akhurst, 2006; Wahab et al., 2000). Previously, we reported that TIP39 is expressed in both the epidermis and differentiated subcutaneous adipocytes and that it regulates intracellular calcium and affects keratinocyte differentiation (Sato et al., 2016). Furthermore, TIP39 up-regulates expression of the *FN1, MMP13,* and *COL1A2* genes in PTH2R-overexpressing chondrocytes (Panda et al., 2009). Collagen and matrix metalloproteases (MMPs) also act in the inflammatory and remodeling phases of wound healing (Brett, 2008). Based on these results, we predicted that TIP39-PTH2R signaling may affect dermal ECM and keratinocyte migration and thereby enhance wound repair. In this study, we hypothesized that in addition to the effects previously shown on keratinocytes, TIP39-PTH2R signaling may also influence wound repair through action on the production of decorin and other ECM components by fibroblasts and adipocytes in the dermis.

RESULTS

TIP39 enhances wound repair

To investigate the effects of TIP39 on mouse excisional wound repair, we performed daily injections of 250 ng TIP39 in the skin of mice and observed significantly enhanced closure on days 2 and 4 compared with vehicle injections (Figure 1a, and see Supplementary Figure S1a online). Similarly, TIP39-knockout mice ($Tip39^{-/-}$) showed a delayed rate of closure from days 2 through 8 (Figure 1b and c). Van Gieson staining of day 7 wound samples from $TIP39^{-/-}$ and littermate control heterozygous mice ($TIP39^{+/-}$) showed that collagen fiber bundles in $TIP39^{-/-}$ wounds were thicker than in $TIP39^{+/-}$ wounds (Figure 1d, and see Supplementary Figure S1b). Furthermore, wound re-epithelialization as measured in a splinted-wound model also suggested that re-epithelialization of $TIP39^{-/-}$ wounds was delayed compared with their heterozygous controls (Figure 1e and f, and see Supplementary Figure S1d).

PTH2R signaling regulates the ECM

To understand how the presence of TIP39 or its receptor might influence wound repair, we next investigated the effects of PTH2R signaling in several cultured cell types, including keratinocytes, endothelial cells, fibroblasts, and adipocytes. Both TIP39 and PTH2R expression were highest in adipocytes (Figure 2a). Transfection of a small interfering RNA (siRNA) targeting PTH2R into human fibroblast-like adipocyte precursor cells and adipocytes was effective at suppressing PTH2R gene expression by more than 90% for both cell types (Figure 2b, and see Supplementary Figure S1e), and whole transcriptome analysis by RNA sequencing showed that PTH2R silencing significantly down-regulated 46 genes in fibroblasts and 252 genes in differentiated adipocytes (Figure 2c). Gene ontology enrichment analysis showed that PTH2R silencing had strong effects on the regulation of ECM in fibroblasts (Figure 2d). Figure 2e and f illustrates significantly down-regulated genes by gene ontogeny analysis: 0030198 (ECM organization). We focused on *DCN* and *COL1A1* for the rest of this study, because type I collagen is highly abundant in the skin and decorin is well known to modulate the regularity of collagen fibrils, is related to skin fragility (Birk and Silver, 1984; Danielson et al., 1997; Scott and Orford, 1981), and may therefore be relevant to the wound healing phenotype observed in Figure 1.

TIP39 enhances the production of decorin from fibroblasts in 3D collagen gels

$TIP39^{-/-}$ mice showed less decorin and MMP13 mRNA expression compared with wounded skin from heterozygous littermates (Figure 3a, and see Supplementary Figure S1c). Because fibroblasts produce more decorin when incubated in 3D type I collagen gels (Lee et al., 2004), we established a 3D collagen culture model in which the mouse fibroblast cell line, 3T3-L1, could be differentiated into adipocytes (see Supplementary Figure S2a online). Differentiation medium, which contains dexamethasone, insulin, and isobutyl methylxanthine, was added to the 3D cultures from 2 days after gel formation. Differentiation was confirmed by up-regulation of *Adipoq* (see Supplementary Figure S2d) and by perilipin expression (see Supplementary Figure S2c). TIP39 suppressed *Adipoq* expression from days 2 through 6 but had no effect on day 7 (see Supplementary Figure S2e). Decorin expression was suppressed by adipocyte differentiation (see Supplementary

Figure S2f), but TIP39 increased decorin production in both undifferentiated fibroblasts and adipocytes in 3D collagen gels (Figure 3b and c).

TIP39 phosphorylates CREB and induces decorin transcription

We next investigated whether TIP39 might affect decorin production via the phosphorylation of CREB in mouse fibroblasts. TIP39 (1.5 μmol/L) increased phosphorylated CREB (pCREB) in the nuclear fraction within 15 minutes after stimulation (Figure 4a and b). Glyceraldehyde 3-phosphate dehydrogenase was used as a housekeeping protein (loading control) for the cytoplasmic fraction, and lamin B was used for the nuclear fraction. Figure 4c shows immunostaining of pCREB (green) and nuclei (blue) after stimulation with 1 μmol/L TIP39. As in Figure 4a, TIP39 induced the translocation of pCREB into the nucleus 15 minutes after stimulation (Figure 4d). TIP39 treatment also resulted in accumulation of decorin in a perinuclear location within 4 hours after TIP39 addition (Figure 4e).

Effects of TIP39 on adipocyte GAGs

As a PG, decorin typically contains CS GAG side chains in the form of dermatan sulfate linked to its N-terminal region, and it also has three potential sites for N-glycosylation in its protein core (Edwards, 2012; Seo et al., 2005). Monosaccharide composition analysis of the supernatant from differentiated adipocytes grown as monolayers showed that they mainly secreted disaccharides consistent with CS/dermatan sulfate (Figure 5a and b). Comparison of GAG production by gel electrophoresis and selective enzymatic digestion techniques of pre-adipocyte fibroblasts and adipocytes showed that 3D collagen gels containing undifferentiated fibroblasts produced yellow-stained material that was digested by heparinase, indicative of heparan sulfate (HS) (Figure 5c, lanes A and B). Production of these materials was clearly reduced in gels containing differentiated adipocytes, which instead mainly produced purple-stained materials that were digested by chondroitinase ABC (Figure 5c, lanes C and D). Thus, undifferentiated fibroblasts mainly produced HS, and differentiated adipocytes mainly produced CS. These changes in GAG composition suggest that GAGs may have an important role in adipocyte differentiation.

We next investigated the expression of various genes encoding HS or CS core proteins (Sarrazin et al., 2011) by quantitative PCR assays (Figure 5d). Adipocyte differentiation down-regulated the expression of *Agrn, Gpc1,* and *Gpc2,* known core proteins of HS. TIP39 significantly increased the expression of *Dcn* in fibroblast and *Tgfbr3* in adipocyte; both are known to contain CS (Figure 5d).

The lack of PTH2R signaling suppresses decorin expression in the mouse dermis

Finally, we investigated the expression of decorin in PTH2R-deficient murine skin. *Pth2r*$^{-/-}$ dermis expressed lower levels of decorin, as determined by immunofluorescence staining (Figure 6a). To quantify decorin expression in the mouse dermis and subcutaneous tissue, we separated epidermis by 0.5 mol/L ammonium thiocyanate treatment. Decorin gene expression was suppressed in *Pth2r*$^{-/-}$ dermis and subcutaneous tissue (Figure 6b). Western blotting data showed that decorin protein expression was also suppressed (Figure 6c). Chondroitinase ABC digestion reduced the size of decorin from approximately 65 kDa to 50 kDa (Figure 6c, right lane). Transmission electron microscopy of collagen fibrils in the *Pth2r*

$^{-/-}$ reticular dermis identified irregular collagen fibrils in these mice (Figure 6d) that are similar to those previously seen in decorin-deficient mouse skin (Danielson et al., 1997). Furthermore, skin hardness measurements of *Pth2r*$^{-/-}$ mice showed that the overall compressibility of the skin from mice lacking the TIP39 receptor is softer than wild-type mice (Figure 6e).

DISCUSSION

The study of GAGs and PGs has improved our understanding of cellular proliferation, differentiation, migration, and wound healing (Trowbridge and Gallo, 2002). We showed in this study that TIP39 and PTH2R induced decorin expression in the dermis and appear to influence the structural organization of the ECM. These effects were associated with improved wound repair upon addition of TIP39 and deficient wound repair in the absence of either TIP39 or PTH2R. Because decorin regulates collagen fibrillogenesis by interacting with collagen triple helices to regulate spacing within fibrils (Edwards, 2012; Weber et al., 1996) and a lack of decorin results in increased skin fragility and deficient wound repair because of these abnormal collagen fibrils (Danielson et al., 1997), the phenotypes observed by altering the TIP39 signaling pathway are consistent with an important role for TIP39 in regulation of decorin. To our knowledge this is the first observation that a member of the PTH family has a direct influence on ECM production in the dermis.

Analysis of the transcriptional response of fibroblasts and adipocytes after the silencing of *PTH2R*, after the addition of TIP39, in *Pth2r*$^{-/-}$ mice, and in a previous study of chondrocytes (Panda et al., 2009) all strongly support the conclusion that PTH2R signaling can influence the production of decorin, collagen, MMPs, tissue inihibitors of metalloproteinase, and PGs. Addition of synthetic TIP39 peptide resulted in the phosphorylation of CREB, an effect previously attributed to stimulation of the $G\alpha_s$–adenylyl cyclase–cyclic adenosine monophosphate pathway and a known factor in the control of decorin expression. We also showed that the expression of *MMP13* was strongly increased after wounding. MMP13 degrades collagen fibrils and contributes to remodeling wound tissue. However, the lack of TIP39 suppressed MMP13 production despite wounding. A previous report showed that PTH2R signaling directly down-regulates the expression of SOX9 and increases MMPs (Panda et al., 2009); our TIP39 knockout data support this report.

Our data of decreased rate of closure of splinted wounds in TIP39$^{-/-}$ mice suggest that the wound repair phenotype in part involves epithelial closure (Figure 1f, and see Supplementary Figure S1d), but this effect may also be due to an influence on the dermis. A direct effect on the epidermis is supported by our previously reported observations that PTH2R can influence calcium homeostasis and differentiation in keratinocytes and that TIP39 increases intracellular 4 °C. Quantitative PCR data are means ± standard error of the mean, n = 4. **P* < 0.05 (Student *t* test). (**d**) Reticular dermal collagen fibrils were observed by transmission electron microscopy in *Pth2r*$^{+/+}$ or *Pth2r*$^{-/-}$ mice. Scale bars = 100 nm. Yellow arrows and asterisks mark irregular collagen fibrils observed in *Pth2r*$^{-/-}$ mice. (**e**) Skin hardness of *Pth2r*$^{-/-}$ mice was measured by a Mitutoyo durometer (Mitutoyo, Aurora, IL). ***P* < 0.01 (Student *t* test). PTH2R, parathyroid hormone second receptor. calcium in

keratinocytes (Sato et al., 2016). Keratinocyte migration is stimulated by increased intracellular calcium and the nuclear factor of activated T-cell proteins, a family of Ca^{2+}-activated transcription factors (Brun et al., 2014; Fang et al., 1998; Jauliac et al., 2002; O'Connor et al., 2007). Thus, part of the wound repair phenotype we observed may be due to a direct effect of TIP39 on keratinocytes. However, GAGs and MMPs from the dermis may also indirectly influence keratinocyte migration. Thus, an indirect effect on epithelial closure due to an influence of TIP39 signaling on the dermis is also possible. Taken together, our current and previously reported observations support the conclusion that TIP39-PTH2R signaling has an important influence on the function of both the epidermis and dermis. These effects of TIP39 and PTH2R point toward an important, multifaceted role in wound healing.

Our collagen gel cultures showed greatly increased decorin expression and supported prior observations of the importance of the 3D environment to model decorin expression in fibroblasts (Lee et al., 2004). This supported the phenotype observed in *Pth2r*$^{-/-}$ mice, in which PTH2R deficiency suppressed decorin expression in the dermis and subcutaneous tissue. Our findings also suggest that GAGs may play a role in adipocyte differentiation. Adipocyte differentiation clearly decreased the expression of various PG genes compared with undifferentiated fibroblasts, and the main type of GAG produced was changed from HS to CS in the 3D collagen gels.

The role of the ECM, decorin, and GAG in adipocyte differentiation is poorly understood. Hyaluronan, an unsulfated GAG, has been suggested to influence adipocyte differentiation (Ji et al., 2014). We observed that the expression of various PGs decreased with adipocyte differentiation in the 3D collagen gels compared with undifferentiated fibroblasts. It is tempting to speculate that this reflects a shift in cell phenotype from a fibroblast dedicated to collagen matrix assembly to an adipocyte that does not require a mechanically strong ECM yet needs to accumulate lipid and also contribute to fighting infection (Zhang et al., 2015). Thus, activation of PTH2R could be predicted to drive an increase in dermal fibrosis and a decrease in adipogenesis.

In summary, this study shows that TIP39-PTH2R signaling regulates decorin, a major component of the ECM, and influences the structure of the dermis and the process of wound repair in mice. These observations open a new avenue of investigation that may be relevant to control of human dermal reorganization in processes such as development, aging, and wound repair.

MATERIALS AND METHODS

Recombinant peptides and antibodies

TIP39 peptides were obtained from Bachem Americas (Torrance, CA). Goat anti-decorin (R&D, Minneapolis, MN), rabbit anti-CREB (Abcam, Cambridge, MA), rabbit anti-pCREB (Abcam), rabbit anti-laminB1 (Abcam), goat anti-perilipin (Abcam), goat anti-actin (Santa Cruz, Dallas, TX), and rabbit anti-glyceraldehyde 3-phosphate dehydrogenase (Abcam) were used as primary antibodies for immunoblotting or immunostaining. Alexa Fluor 488- or 594-conjugated donkey IgG (Thermo Fisher Scientific, Waltham, MA) were used as secondary antibodies for immunostaining.

Mice

6- to 18-week-old female C57BL/6, *Pth2r*$^{-/-}$ *Tip39*$^{-/-}$ mice and their littermates were housed at the University Research Center at the University of California, San Diego. *Pth2r*$^{-/-}$ and *Tip39*$^{-/-}$ mice were obtained from Ted B. Usdin (Nation Institute of Mental Health, Bethesda, MD). All animal experiments were approved by the University of California, San Diego Institutional Animal Care and Use Committee.

Fibroblast-like precursor cells in monolayer and 3D collagen culture

Primary human subcutaneous fibroblast-like precursor cells (pre-adipocytes) were obtained from Cell Applications (San Diego, CA), and primary mouse fibroblast/preadipocyte cell line 3T3-L1 was purchased from ATCC (Manassas, VA) grown in preadipocyte growth medium (Cell Applications) for up to seven passages under standard tissue culture conditions previously described (Zhang et al., 2015). Cells were cultured until 80–90% confluence, and then adipocyte differentiation medium (Cell Applications) was replaced. Primary human keratinocytes and endothelial cells are cultured as previously described (Adase et al., 2016). For construction of 3T3-L1–containing 3D collagen plugs, type I collagen (Thermo Fisher Scientific) was solubilized in sterile-filtered Milli-Q water (EMD Millipore, Billerica, MA) to a stock concentration of 5 mg/ml. The detailed methods of 3T3-L1 collagen plug production are described by Borkowski et al. (2013) and Simpson et al. (2010). Gel formation occurred over 30 minutes at 37 °C, after which the gels were released from well sides with a pipette tip and from the bottom of the well with minimal shaking of the plate. After gel formation, 3 ml of 10% fetal bovine serum DMEM (Thermo Fisher Scientific) was added on the 3D collagen plug. For inducing adipocyte differentiation, the outside medium was changed from 10% fetal bovine serum-contained DMEM to adipocyte differentiation medium at 48 hours after gel formation. 1 μmol/L TIP39 was mixed in both collagen plugs and added to media.

GAG and PG isolation by anion exchange chromatography

3T3-L1 was seeded on 10-cm dishes and then cultured until 80–90% confluency. Adipocyte differentiation was induced for 3 days with or without 5 μmol/L TIP39. The 30-ml supernatant of each group was concentrated by Amicon Ultra 10K filter (Millipore, Billerica, MA). For digestion of the protein, the supernatant was incubated overnight with 0.1 mg/ml protease (Sigma-Aldrich, St. Louis, MO) at 37 °C, followed by purification by anion exchange chromatography using DEAE Sephacel (GE Healthcare, Chicago, IL). Columns were washed with a low-salt buffer (150 mmol/L NaCl in 50 mmol/L sodium acetate, pH 6.0) and eluted with 1 mol/L NaCl. GAGs were desalted by PD10 (GE Healthcare). The detailed method is described in the manual of GAG Release and Purification (Glycobiology Research Training Center, n.d.) and Muto et al. (2014). For isolation of GAGs from 3D 3T3-L1 collagen gels, the plugs were dissolved in 3 mL radio-immunoprecipitation assay buffer for 10 minutes in a 60 °C water bath. The dissolved samples were vortexed at the highest speed and then centrifuged for 15 minutes at 15,000*g* at 4 °C. Those supernatants were used for GAG isolation.

Quantitative real-time PCR

Total RNA from mouse tissue samples and cultured keratinocytes was extracted, and cDNA was synthesized as previously described (Sato et al., 2016). TaqMan gene expression assays (Thermo Fisher Scientific) were used to analyze expressions of mouse decorin (gene symbol, *Dcn*; assay ID, Mm00514535_m1), mouse adiponectin (gene symbol, *Adipoq*; assay ID, Mm00456425_m1), mouse syn-decan1 (gene symbol, *Sdc1*; assay ID, Mm00448918_m1), mouse syndecan2 (gene symbol, *Sdc2*; assay ID, Mm04207492_m1), mouse syndecan4 (gene symbol, *Sdc4*; assay ID, Mm00488527_m1), mouse aggrecan (gene symbol, *Acan*; assay ID, Mm00545794_m1), mouse agrin (gene symbol, *Agrn*; assay ID, Mm01264855_m1), mouse glypican1 (gene symbol, *Gpc1*; assay ID, Mm01264855_m1), mouse glypican2 (gene symbol, *Gpc2*; assay ID, Mm00549650_m1), mouse perlecan (gene symbol, *Hspg2*; assay ID, Mm01181173_g1), and mouse β-glycan (gene symbol, *Tgfbr3*; assay ID, Mm00803538_m1), as described by the manufacturer's instructions. Mouse β-actin (gene symbol, *Actb*; assay ID, Mm00607939_s1) was used as an internal control to validate RNA for each sample. Primer sequences of human PTH2 receptor, TIP39, and β-actin were as follows: *PTH2R* forward: 5′-CAGTTGGGC ATGACACAAGG-3′, *PTH2R* reverse: 5′-ACACAAAGAAACCCT GAAAGGA-3′; *PTH2* forward: 5′-CCCCTTTCTGGTTCTCCACAG-3′, *PTH2* reverse: 5′-GCATGTACGAGTTCAGCCA-3′; *ACTB* forward: 5′-GCAAATGCTTCTAGGCGGAC-3′, *ACTB* reverse: 5′-CGCATCTCA TATTTGGAATGACT-3′. Each mRNA expression was calculated as the relative expression to β-actin mRNA, and all data are presented as fold change against each control (mean of nonstimulated cells).

Protein extraction and immunoblotting

Samples were lysed in radio-immunoprecipitation assay buffer as previously described (Sato et al., 2016). Protein concentrations were measured by BCA protein assay kit (Thermo Fischer Scientific). For immunoblotting, 10 μg of protein was separated on a 10% Tris-Glycine precast gel (Bio-Rad, Hercules, CA), transferred to a polyvinylidene fluoride membrane (Bio-Rad), followed by immunoblotting using indicated primary antibodies, followed by fluorescent secondary antibodies (LICOR, Lincoln, NE) and imaging using fluorescent Odyssey System (LICOR). Densitometry was performed on scanned immunoblot images using the ImageJ software (National Institutes of Health, Bethesda, MD) based on the measurement of the relative intensity. Values were further normalized to CREB levels in the respective blots.

Wound healing model

Two 6-mm full-thickness excisional wounds were created on the shaved dorsal surface of 8-week-old female C57BL/6 wild-type, *TIP39*$^{-/-}$, and *TIP39*$^{+/-}$ mice under sterile conditions. Wound margins were then injected with or without TIP39 (250 ng/50 μl, 1.11 μmol/L) every 24 hours for 10 days after injury and photographed every 48 hours over that period, and the wound area was manually traced by placing a transparent film over the wound and tracing the outline with a permanent marker. The method of wound measure has been described at (Ma et al., 2015). The tracing was then scanned and measured using an image analysis program (Image J Software, version 1.48). Three mice, each with two wounds (a total of six

wounds) were studied in each treatment arm, and their rate of closure was analyzed. The study protocol included standard wound care as per Institutional Animal Use and Care Committee guidelines. The splinted wound model was modified from Galiano et al., 2004. A sterile 4-mm punch biopsy tool was used to create paired full-thickness wounds extending through the panniculus carnosus. A donut-shaped splint with outer diameter of 10 mm and inner diameter of 6mm was fashioned from a 0.5-mm–thick silicone sheet (Grace Bio-Laboratories, Bend, OR). The splint was placed so that the wound was fully visible in the center, and interrupted 5-0 nylon sutures (Ethicon, Inc., Somerville, NJ) were used to fix the splint to the skin. The animals were monitored throughout recovery from anesthesia and housed individually in the University of California–San Diego vivarium.

Immunofluorescence staining of cultured cells

Cells were fixed in −20 °C cold methanol for 10 minutes then blocked with phosphate buffered saline containing 5% donkey serum at room temperature for 30 minutes. For sectioning of 3D collagen 3T3-L1, collagen plug was embedded in Optimal Cutting Temperature compound (Sakura Finetek USA, Torrance, CA) as previously described (Lee et al., 2004). Sectioning was performed at University of California–San Diego Moores Histology Core (La Jolla, CA). The detailed immunostaining method has been described (Sato et al., 2016). Anti-pCREB, anti-perilipin, anti-decorin, and Alexa Fluor 488- or 594-conjugated donkey IgG (Thermo Fisher Scientific) were used at 1μg/ml. Cover slips were mounted using ProLong Gold Antifade Reagent with DAPI (Thermo Fisher Scientific). Images were captured using a BX41 microscope (Olympus, Center Valley, PA).

Immunofluorescence for paraffin-embedded sections

The skin tissue samples were fixed in 10% formalin for 24 hours. Paraffin embedding and sectioning were performed at University of California–San Diego Moores Histology Core. The 5-μm paraffin sections were deparaffinized and rehydrated before heat-induced antigen retrieval was performed in 10 mmol/L citrate buffer (pH 6.0) for 15 minutes at 121 °C (250 °F). Immunostaining was performed as previously described (Sato et al., 2016). Anti-decorin, anti-PTH2/TIP39, and Alexa Fluor 488- or 594-conjugated antibodies (donkey IgG) were used at 1μg/ml.

Van Gieson staining for paraffin-embedded sections

Van Gieson staining was performed at University of California–San Diego Moores Histology Core. Deparaffinized slides were stained using Elastic Stain Kit (Sigma-Aldrich) as its protocol (procedure no. HT25). Elastic fibers and nuclear components are stained blue to black, collagen is red, and muscle/other tissues are yellow.

RNA knockdown

Control and PTH2R Silencer Select siRNA were purchased from Thermo Fisher Scientific. siRNA transfection was performed by manufacturer's instructions of Lipofectamine RNAiMAX (MAN0007836, Thermo Fisher Scientific). Human fibroblast-like precursor cells were seeded on 24-well plates (fibroblast group: 2.0×10^4/well, adipocyte group: 5.0×10^4/well) and then incubated overnight. At day 0, siRNA complex was transfected into cells

with or without adipocyte differentiation medium. Both siRNA and culture medium were replaced at day 3. All samples were harvested at 5 days after transfection.

RNA sequencing analysis

The detailed RNA sequencing method is described by Adase et al. (2016). RNA quality was checked using the R6K screen tape with an Agilent 2200 TapeStation (Agilent Technologies, Santa Clara, CA). RNA sequencing libraries were prepared using the TruSeq Stranded mRNA (Illumina, San Diego, CA) and sequenced with the HiSeq2500, HighOutput v4 system (Illumina). All those processes were performed at the IGM Genomics Center, University of California–San Diego, La Jolla, CA. Gene analysis used Partek Gene Specific Analysis run on the gene level with the following changes: Lowest maximum coverage = 1, Poisson = True, and trimmed mean of M values normalization. Gene filters used had a false discovery rate of less than 0.1. Hierarchical clustering and gene ontology enrichment were performed using these filters with Partek flow software.

Durometer measurements

Durometer measurements were made using a handheld dial durometer (HARDMATIC HH-300 Shore A; Mitutoyo, Kanagawa, Japan). This durometer is provided with a peak retaining hand for error-free reading. Five consecutive durometer measurements were taken on each of five mice dorsal skins under anesthesia using isoflurane gas (2–5%, flow rate = 1 L/minute).

Raw and processed data discussed in this publication have been deposited in NCBI's Gene Expression Omnibus and are accessible through GEO Series accession number GSE89647 (https://www.ncbi.nlm.nih.gov/geo/query/acc.cgi?token=kpgpmoeqrhwzvyz&acc=GSE89647).

Supplementary Material

Refer to Web version on PubMed Central for supplementary material.

Acknowledgments

The authors would like to thank all the members of the Gallo laboratory for the input and stimulating conversations. We thank Y. Jones at the UCSD EM Core for processing samples and helpful discussion of electron microscopy images. We thank UCSD Histology Core Facility for sectioning, hematoxylin and eosin staining, and van Gieson staining of paraffin samples.

This work was supported in part by P01HL057345 and P01HL107150 to RLG and the UCSD Dermatologist Investigator Training Program 1T32AR062496 (JAS, CA).

Abbreviations

3D	three dimensional
CS	chondroitin sulfate
ECM	extracellular matrix
GAG	glycosaminoglycan

HS	heparan sulfate
MMP	matrix metalloprotease
pCREB	phosphorylated CREB
PG	proteoglycan
PTH	parathyroid hormone
PTH2R	parathyroid hormone second receptor
siRNA	small interfering RNA

References

Adase CA, Borkowski AW, Zhang LJ, Williams MR, Sato E, Sanford JA, et al. Non-coding double-stranded RNA and antimicrobial peptide LL-37 induce growth factor expression from keratinocytes and endothelial Cells. J Biol Chem. 2016; 291:11635–46. [PubMed: 27048655]

Akhurst RJ. A sweet link between TGFbeta and vascular disease? Nat Genet. 2006; 38:400–1. [PubMed: 16570059]

Atfi A, Baron R. PTH battles TGF-beta in bone. Nat Cell Biol. 2010; 12:205–7. [PubMed: 20190828]

Birk DE, Silver FH. Collagen fibrillogenesis in vitro: comparison of types I, II, and III. Arch Biochem Biophys. 1984; 235:178–85. [PubMed: 6437334]

Borkowski AW, Park K, Uchida Y, Gallo RL. Activation of TLR3 in keratinocytes increases expression of genes involved in formation of the epidermis, lipid accumulation, and epidermal organelles. J Invest Dermatol. 2013; 133:2031–40. [PubMed: 23353987]

Brett D. A review of collagen and collagen-based wound dressings. Wounds. 2008; 20:347–56. [PubMed: 25941895]

Brun C, Demeaux A, Guaddachi F, Jean-Louis F, Oddos T, Bagot M, et al. T-plastin expression downstream to the calcineurin/NFAT pathway is involved in keratinocyte migration. PLoS One. 2014; 9:e104700. [PubMed: 25226517]

Danielson KG, Baribault H, Holmes DF, Graham H, Kadler KE, Iozzo RV. Targeted disruption of decorin leads to abnormal collagen fibril morphology and skin fragility. J Cell Biol. 1997; 136:729–43. [PubMed: 9024701]

Edwards IJ. Proteoglycans in prostate cancer. Nat Rev Urol. 2012; 9:196–206. [PubMed: 22349653]

Fang KS, Farboud B, Nuccitelli R, Isseroff RR. Migration of human keratinocytes in electric fields requires growth factors and extracellular calcium. J Invest Dermatol. 1998; 111:751–6. [PubMed: 9804333]

Galiano RD, Michaels JT, Dobryansky M, Levine JP, Gurtner GC. Quantitative and reproducible murine model of excisional wound healing. Wound Repair Regen. 2004; 12:485–92. [PubMed: 15260814]

Gallo RL, Ono M, Povsic T, Page C, Eriksson E, Klagsbrun M, et al. Syndecans, cell surface heparan sulfate proteoglycans, are induced by a proline-rich antimicrobial peptide from wounds. Proc Natl Acad Sci USA. 1994; 91:11035–9. [PubMed: 7972004]

Glycobiology Research and Training Center. [accessed 18 May 2017] GAG release and purification. n.d. http://glycotech.ucsd.edu/protocols/12_GAG%20Release%20and%20Analysis_Rev3.pdf

Jarvelainen H, Puolakkainen P, Pakkanen S, Brown EL, Hook M, Iozzo RV, et al. A role for decorin in cutaneous wound healing and angiogenesis. Wound Repair Regen. 2006; 14:443–52. [PubMed: 16939572]

Jauliac S, Lopez-Rodriguez C, Shaw LM, Brown LF, Rao A, Toker A. The role of NFAT transcription factors in integrin-mediated carcinoma invasion. Nat Cell Biol. 2002; 4:540–4. [PubMed: 12080349]

Ji E, Jung MY, Park JH, Kim S, Seo CR, Park KW, et al. Inhibition of adipogenesis in 3T3-L1 cells and suppression of abdominal fat accumulation in high-fat diet-feeding C57BL/6J mice after downregulation of hyaluronic acid. Int J Obes. 2014; 38:1035–43.

Lee PH, Trowbridge JM, Taylor KR, Morhenn VB, Gallo RL. Dermatan sulfate proteoglycan and glycosaminoglycan synthesis is induced in fibroblasts by transfer to a three-dimensional extracellular environment. J Biol Chem. 2004; 279:48640–6. [PubMed: 15347686]

Ma GS, Aznar N, Kalogriopoulos N, Midde KK, Lopez-Sanchez I, Sato E, et al. Therapeutic effects of cell-permeant peptides that activate G proteins downstream of growth factors. Proc Natl Acad Sci USA. 2015; 112:E2602–10. [PubMed: 25926659]

Muto J, Morioka Y, Yamasaki K, Kim M, Garcia A, Carlin AF, et al. Hyaluronan digestion controls DC migration from the skin. J Clin Invest. 2014; 124:1309–19. [PubMed: 24487587]

Naylor EC, Watson RE, Sherratt MJ. Molecular aspects of skin ageing. Maturitas. 2011; 69:249–56. [PubMed: 21612880]

O'Connor RS, Mills ST, Jones KA, Ho SN, Pavlath GK. A combinatorial role for NFAT5 in both myoblast migration and differentiation during skeletal muscle myogenesis. J Cell Sci. 2007; 120:149–59. [PubMed: 17164296]

Panda D, Goltzman D, Juppner H, Karaplis AC. TIP39/parathyroid hormone type 2 receptor signaling is a potent inhibitor of chondrocyte proliferation and differentiation. Am J Physiol Endocrinol Metab. 2009; 297:E1125–36. [PubMed: 19706789]

Qiu T, Wu X, Zhang F, Clemens TL, Wan M, Cao X. TGF-beta type II receptor phosphorylates PTH receptor to integrate bone remodelling signalling. Nat Cell Biol. 2010; 12:224–34. [PubMed: 20139972]

Ritter SL, Hall RA. Fine-tuning of GPCR activity by receptor-interacting proteins. Nat Rev Mol Cell Biol. 2009; 10:819–30. [PubMed: 19935667]

Rostand KS, Esko JD. Microbial adherence to and invasion through proteoglycans. Infect Immun. 1997; 65:1–8. [PubMed: 8975885]

Sarrazin S, Lamanna WC, Esko JD. Heparan sulfate proteoglycans. Cold Spring Harb Perspect Biol. 2011; 3:a004952. [PubMed: 21690215]

Sato E, Muto J, Zhang LJ, Adase C, Sanford JA, Takahashi T, et al. The parathyroid hormone second receptor PTH2R, and its ligand tuberoinfundibular peptide of 39 residues TIP39, regulate intracellular calcium and influence keratinocyte differentiation. J Invest Dermatol. 2016; 136:1449–59. [PubMed: 27000502]

Schaefer L, Schaefer RM. Proteoglycans: from structural compounds to signaling molecules. Cell Tissue Res. 2010; 339:237–46. [PubMed: 19513755]

Schmidt BA, Horsley V. Intradermal adipocytes mediate fibroblast recruitment during skin wound healing. Development. 2013; 140:1517–27. [PubMed: 23482487]

Scott JE, Orford CR. Dermatan sulphate-rich proteoglycan associates with rat tail-tendon collagen at the d band in the gap region. Biochem J. 1981; 197:213–6. [PubMed: 7317031]

Seo NS, Hocking AM, Hook M, McQuillan DJ. Decorin core protein secretion is regulated by N-linked oligosaccharide and glycosaminoglycan additions. J Biol Chem. 2005; 280:42774–84. [PubMed: 16258169]

Simpson CL, Kojima S, Getsios S. RNA interference in keratinocytes and an organotypic model of human epidermis. Methods Mol Biol. 2010; 585:127–46. [PubMed: 19908001]

Trowbridge JM, Gallo RL. Dermatan sulfate: new functions from an old glycosaminoglycan. Glycobiology. 2002; 12:117R–25R.

Usdin TB, Hoare SR, Wang T, Mezey E, Kowalak JA. TIP39: a new neuropeptide and PTH2-receptor agonist from hypothalamus. Nat Neurosci. 1999; 2:941–3. [PubMed: 10526330]

Wahab NA, Parker S, Sraer JD, Mason RM. The decorin high glucose response element and mechanism of its activation in human mesangial cells. J Am Soc Nephrol. 2000; 11:1607–19. [PubMed: 10966485]

Weber IT, Harrison RW, Iozzo RV. Model structure of decorin and implications for collagen fibrillogenesis. J Biol Chem. 1996; 271:31767–70. [PubMed: 8943211]

Zhang LJ, Guerrero-Juarez CF, Hata T, Bapat SP, Ramos R, Plikus MV, et al. Innate immunity. Dermal adipocytes protect against invasive *Staphylococcus aureus* skin infection. Science. 2015; 347:67–71. [PubMed: 25554785]

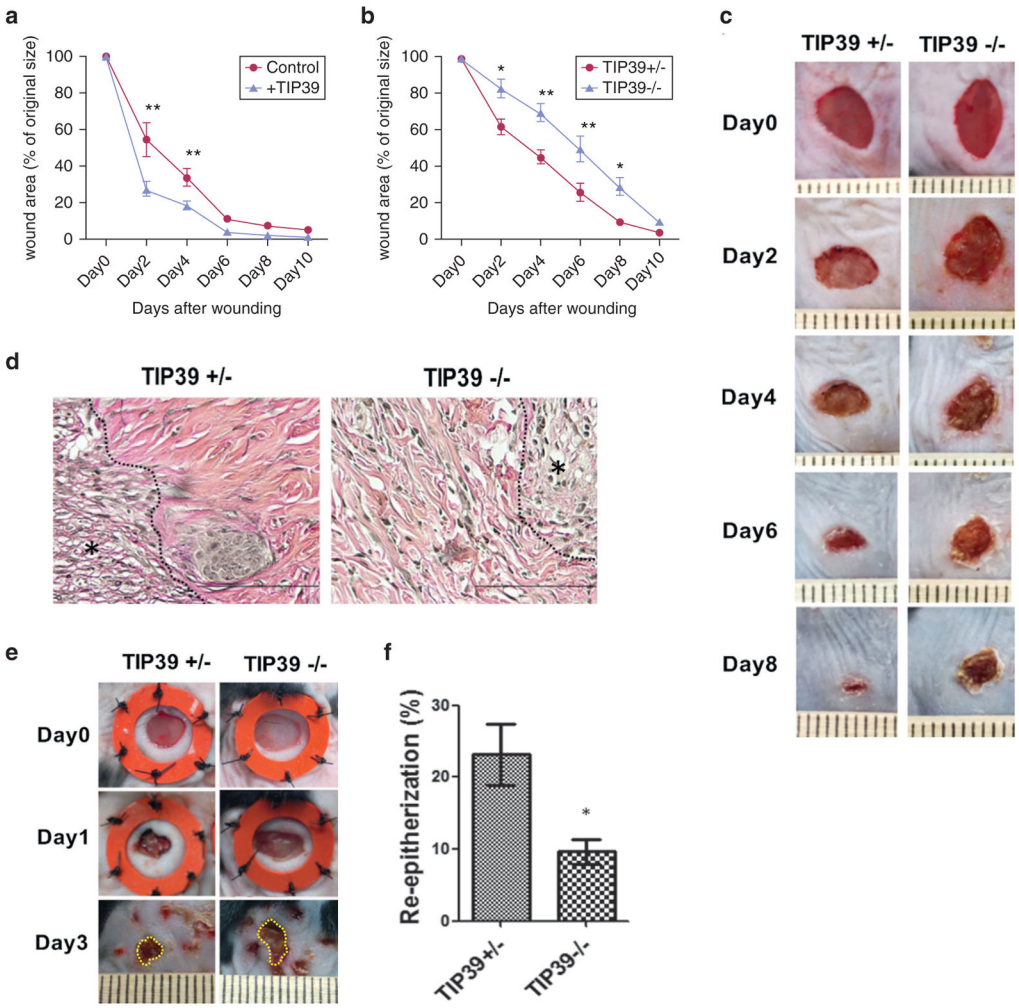

Figure 1. Activation of the PTH2R enhances wound repair

(**a**) Wounds were made on C57BL/6 back skin by 6-mm punch, then injected with 50 μl phosphate buffered saline or 250 ng of TIP39 peptide dissolved in 50 μl phosphate buffered saline. Peptide or phosphate buffered saline were injected to the wound margin daily. Wound closure rate (%) was calculated by Image J software. Data are mean ± standard error of the mean, n = 6, $^{**}P < 0.01$ (two-way analysis of variance with Bonferroni test). (**b**–**d**) Wounds were made on TIP39 knockout ($TIP39^{-/-}$) or heterozygous ($TIP39^{+/-}$) back skin by 6-mm punch. (**b**) Wound closure rate (%) was calculated as in **a**. Data are mean ± standard error of the mean, n = 6, $^{*}P < 0.05$, $^{**}P < 0.01$ (two-way analysis of variance with Bonferroni test.) (**c**) Macro images of the wound healing process. (**d**) Day 7 wounds were stained by van Gieson staining. Collagen bundles are stained red. Asterisk indicates granulation tissue. (**e**) Macro images of splinted wound healing process. Wounds were made on $TIP39^{-/-}$ or $TIP39^{+/-}$ back skin by 4-mm punch. Yellow dotted line shows wound edge. (**f**) Epithelial closure rate of day 3 splint wounds were calculated in histological sections by Image J software. Re-epithelialization (%) = neo-epidermal diameter/wound diameter × 100. $^{*}P < 0.05$ (Student *t* test), n = 4. PTH2R, parathyroid hormone second receptor.

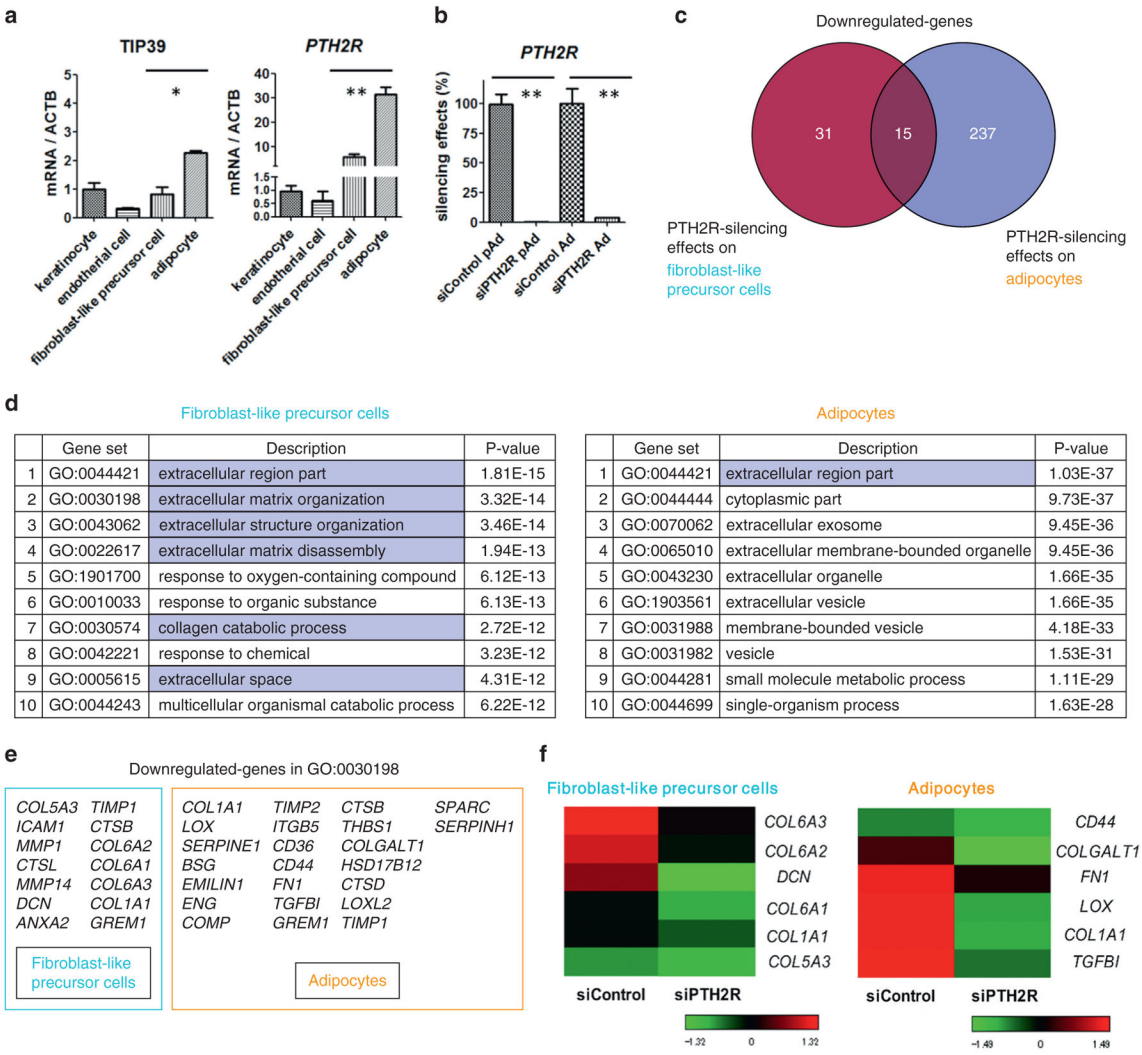

d

Fibroblast-like precursor cells

	Gene set	Description	P-value
1	GO:0044421	extracellular region part	1.81E-15
2	GO:0030198	extracellular matrix organization	3.32E-14
3	GO:0043062	extracellular structure organization	3.46E-14
4	GO:0022617	extracellular matrix disassembly	1.94E-13
5	GO:1901700	response to oxygen-containing compound	6.12E-13
6	GO:0010033	response to organic substance	6.13E-13
7	GO:0030574	collagen catabolic process	2.72E-12
8	GO:0042221	response to chemical	3.23E-12
9	GO:0005615	extracellular space	4.31E-12
10	GO:0044243	multicellular organismal catabolic process	6.22E-12

Adipocytes

	Gene set	Description	P-value
1	GO:0044421	extracellular region part	1.03E-37
2	GO:0044444	cytoplasmic part	9.73E-37
3	GO:0070062	extracellular exosome	9.45E-36
4	GO:0065010	extracellular membrane-bounded organelle	9.45E-36
5	GO:0043230	extracellular organelle	1.66E-35
6	GO:1903561	extracellular vesicle	1.66E-35
7	GO:0031988	membrane-bounded vesicle	4.18E-33
8	GO:0031982	vesicle	1.53E-31
9	GO:0044281	small molecule metabolic process	1.11E-29
10	GO:0044699	single-organism process	1.63E-28

Figure 2. PTH2R signaling influences the extracellular matrix

(**a**) Expression of TIP39 and PTH2R mRNA in various human primary cells. (**b**) PTH2R gene expression was analyzed by quantitative PCR 5 days after silencing of PTH2R expression. (**c**) Silencing effects of PTH2R on fibroblasts or adipocytes were analyzed by RNA sequencing gene profiling. Down-regulated genes with a significant false discover rate (<0.1) are represented. n = 4. (**d**) Top 10 GO terms of PTH2R-silenced fibroblasts and adipocytes. (**e**) Down-regulated genes in GO: 0030198 (extracellular matrix organization). (**f**) Heat map of gene expression in siPTH2R-transfected fibroblasts or adipocytes. Quantitative PCR data are means ± standard error of the mean of biological replicates from n = 3. ** $P < 0.001$ (one-way analysis of variance with Dunnett multiple comparison test). Ad, adipocytes; GO, gene ontology; pAd, fibroblast-like precursor cells; PTH2R, parathyroid hormone second receptor; si, small interfering.

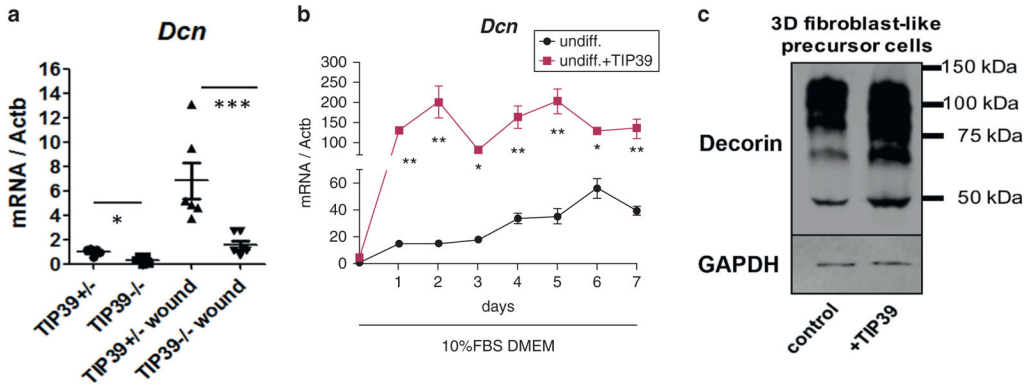

Figure 3. TIP39 increased decorin expression in fibroblast-containing 3D collagen gels

(**a**) Day 0 normal skin and day 10 wound samples from TIP39$^{+/-}$ or TIP39$^{-/-}$ were analyzed by quantitative PCR. Data are mean ± standard error of the mean, n = 6, *$P < 0.05$, ***$P < 0.001$ (one-way analysis of variance with Dunnett multiple comparison test). (**b**) Gene expression of decorin in 3T3-L1 fibroblasts in 3D collagen gels supplied with or without 1 μmol/L TIP39. (**c**) Immunoblotting of decorin in fibroblasts contained-3D collagen gels supplied with or without 1 μmol/L TIP39. 3T3-L1 was cultured in collagen gel for 7 days. Data are means ± standard error of the mean, n = 4. *$P < 0.05$, **$P < 0.01$ (two-way analysis of variance with Bonferroni test). 3D, three dimensional; FBS, fetal bovine serum; GAPDH, glyceraldehyde-3-phosphate dehydrogenase; undiff, undifferentiated.

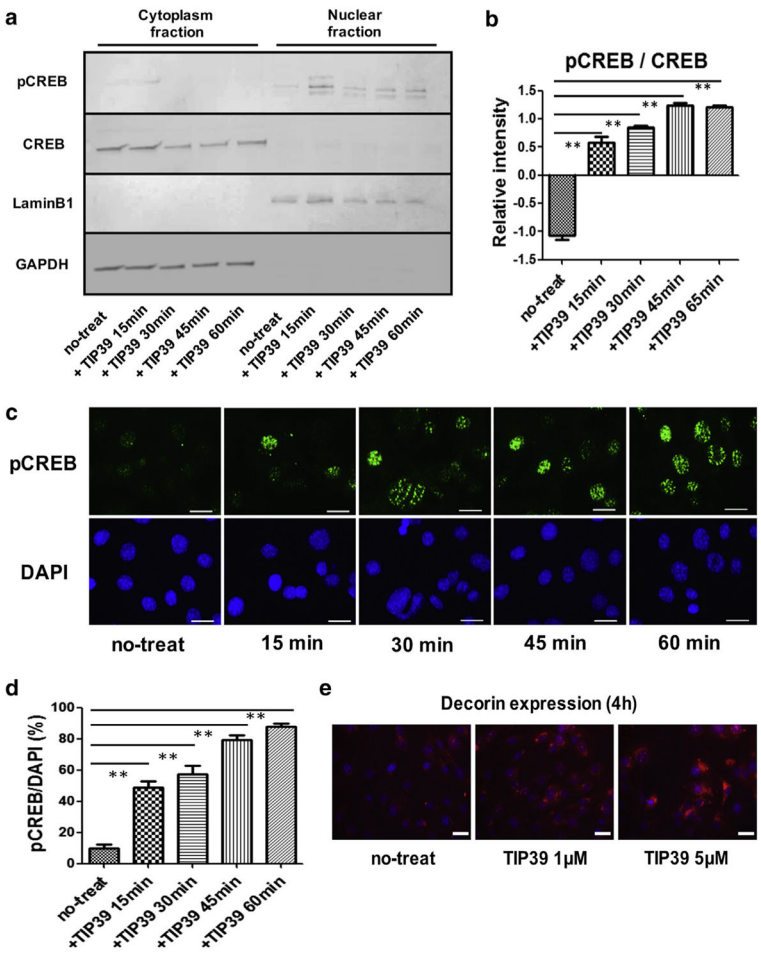

Figure 4. TIP39 induced phosphorylation of CREB in fibroblasts

(**a**) Cytoplasmic and nuclear proteins were isolated from a monolayer of 3T3-L1 cells, which were stimulated by 1.5 μmol/L TIP39 and then analyzed by immunoblotting. (**b**) Relative abundance calculated by Image J software of immunoblot of pCREB/CREB. Data are means ± standard error of the mean, n = 3. (**c**) pCREB in 1μmol/L TIP39-stimulated fibroblasts. Scale bars = 20μm. (**d**) Immunofluorescence staining rate (%) of pCREB (green)/DAPI (blue). Data are means ± standard error of the mean, n = 10. $^{**}P < 0.001$ (one-way analysis of variance with Dunnett multiple comparison test). (**e**) Immunofluorescence staining of decorin (red) with DAPI (blue). GAPDH, glyceraldehyde-3-phosphate dehydrogenase; h, hour; M, mol/L; min, minute; pCREB, phosphorylated CREB.

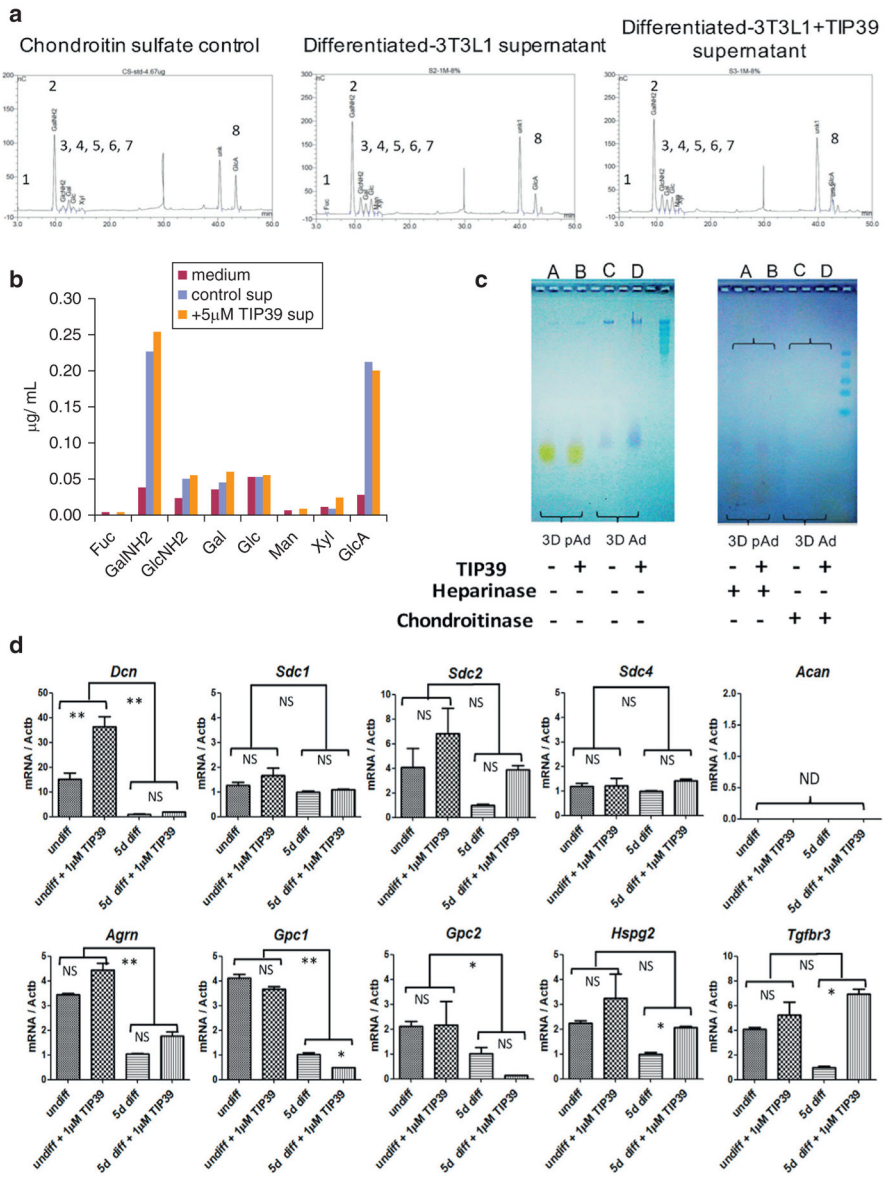

Figure 5. Differentiating adipocytes produce chondroitin sulfate GAG

(**a and b**) Monolayers of 3T3-L1 cells were differentiated for 3 days with or without 5 μmol/L TIP39, and then supernatant was collected from each group. The secreted GAGs were extracted by diethylethanolamine column, and 8% of the GAGs from total samples were used for monosaccharide composition analysis using HPAEC-PAD. (**c**) GAGs were extracted from 3T3-L1–containing collagen gels; 25% of the total samples were used for gel electrophoresis. The right panel shows digested GAGs by 20 mU heparinase 1 and 3 (3D pAd group) or 300 mU chondroitinase ABC (3D Ad group) for 4 hours at 37 °C. The agarose gel was stained by Stains-All (Sigma-Aldrich, St. Louis, MO). 3T3-L1 cells were cultured in collagen gels for 7 days with or without 1 μmol/L TIP39. Adipocyte differentiation was started from 2 days after gel formation. (**d**) mRNA expression of various core proteins of GAGs in 3T3-L1–containing collagen gel. Culture conditions were the same

as in **c**. Data are means ± standard error of the mean, n = 4. *$P < 0.05$, **$P < 0.01$ (one-way analysis of variance with Dunnett multiple comparison test). 3D, three dimensional; Ad, adipocytes; diff, differentiated; GAG, glycosaminoglycan; M, mol/L; ND, no data; NS, not significant; pAd, fibroblast-like precursor cells; sup, supernatant; undiff, undifferentiated.

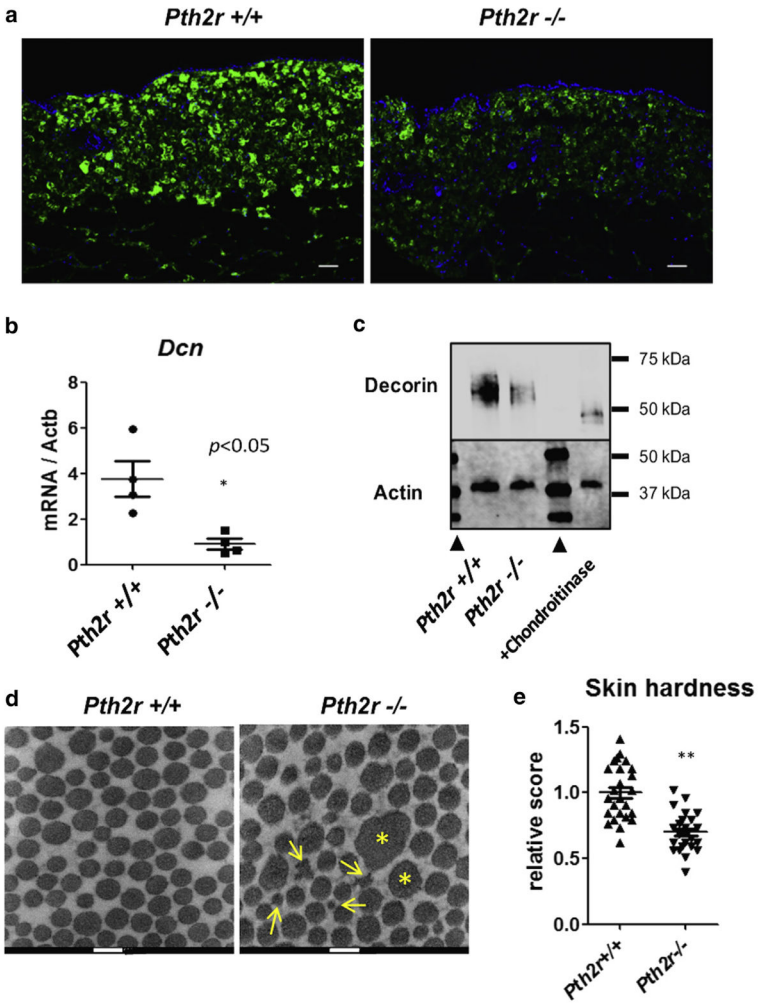

Figure 6. The lack of PTH2R signal decreased decorin production from dermal fibroblasts

(**a**) Immunofluorescence staining of decorin (green) in the skin of *Pth2r*$^{+/+}$ or *Pth2r*$^{-/-}$ mice. Scale bars = 20 μm. Blue is DAPI. (**b**) mRNA expression (quantitative PCR) and (**c**) protein expression (immunoblotting) of decorin in *Pth2r*$^{+/+}$ or *Pth2r*$^{-/-}$ dermis. Arrowheads show protein ladder (700 channel near-infrared detection). Decorin was detected in the 800 channel, and actin was detected in the 700 channel. The right lane of dermis/subcutaneous sample was digested by 300 mU chondroitinase ABC for 3 hours at 37°C. Mouse dermis and subcutaneous tissues were separated from whole skin by 0.5 mol/L ammonium thiocyanate overnight at